Mercapto-benzothiazolyl based ruthenium(ii) borate complexes synthesis and reactivity towards various phosphines

Mohammad Zafar, Ramalakshmi Rongala, Alaka Nanda Pradhan, Kriti Pathak, Thierry Roisnel, Jean-François Halet, Sundargopal Ghosh

Mercapto-benzothiazolyl based ruthenium(II) borate complexes: Synthesis and reactivity towards various phosphines

Mohammad Zafar,[a] Rongala Ramalakshmi,[a] Alaka Nanda Pradhan,[a] Kriti Pathak,[a] Thierry Roisnel,[b] Jean-François Halet,[b] Sundargopal Ghosh*[a]

The synthesis and reactivity of ruthenium complexes containing an anionic boron based ligand, supported by mercapto-benzothiazolyl heterocycles are presented. Specifically, reaction of [(η^6-*p*-cymene)Ru{P(OMe)$_2$OR}Cl$_2$], (**1a**: R = Me; **1b**: R = H) with [H$_2$B(mbz)$_2$]$^-$ (mbz = 2-mercaptobenzothiazolyl) at room temperature afforded a series of borate complexes, namely [(L)Ru{κ^3-H,S,S′-H$_2$B(L)$_2$}P(O)(OMe)(HL)], **2**, [Ru{κ^3-H,S,S′-H$_2$B(L)$_2$}$_2$], **3** and [(κ^2-*N,S*-L)P(OMe)$_3$Ru{κ^3-H,S,S′-H$_2$B(L)$_2$}], **4a**; (L = C$_7$H$_4$NS$_2$). The pivotal feature of **2** is the coordination of the Ru centre with a phosphorus atom of secondary phosphine oxide and mercapto-benzothiazolyl ligands. On the other hand, **3** features dual Ru···H-B interactions between Ru and B-H bonds of [H$_2$B(mbz)$_2$]$^-$. Interestingly, along with **3**, compound [(κ^2-*N,S*-L)P(OPh)$_3$Ru{κ^3-H,S,S′-H$_2$B(L)$_2$}], **4b** (L = C$_7$H$_4$NS$_2$), was isolated upon treatment of the same borate with [(η^6-*p*-cymene)RuCl$_2$P(OPh)$_3$], **1c**, which is stabilized by δ-B-H interactions and one phosphite ligand. Further, compound **3** promptly reacts with P(OR)$_3$ to generate [(OR)$_3$PRu-{κ^2-S,S′-H$_2$B(L)$_2$}{κ^3-H,S,S′-H$_2$B(L)$_2$}], (**5a**: R = Me, **5b**: R = Ph; L = C$_7$H$_4$NS$_2$) by breaking one of the Ru···H-B interactions. Upon heating, compound **5a** converts into [(OMe)$_2$OPRu{κ^2-S,S′-HB(L)$_2$}{κ^3-H,S,S′-H$_2$B(L)$_2$}], **6a** (L = C$_7$H$_4$NS$_2$) by release of methane gas. Compound **6a** is a unique example wherein boron atom of borate ligand is bound to an oxygen atom of the phosphite unit. In contrast, thermolysis of **3** with PR$_2$R′ yielded [Ru{κ^3-H,S,S′-H$_2$B(L$_2$)}(PR$_2$R′)$_2$(L)], (**7a**: R = Me, R′ = Ph; **7b**: R = Ph; R′ = Me; L = C$_7$H$_4$NS$_2$) respectively, revealing incorporation of two triphosphine ligands in the coordination sphere of ruthenium. Density functional theory (DFT) calculations were undertaken to provide an insight into the electronic structures of the complexes.

Introduction

Phosphorus ligands are arguably very important due to their steric properties, basicity as well as diverse substituents.[1,2] Interestingly, these ligands have high tunable stereoelectronic and strong binding characters towards transition metals.[1-3] Consequently, phosphorus-containing ligands are widely utilized in coordination chemistry and catalysis.[4] However, most phosphines are extremely sensitive to moisture, air oxidation and are difficult to handle during the synthesis.[5] To overcome these problems, stable secondary phosphine oxides (SPOs) have received considerable attention recently, even though the first SPO-metal complex was reported in 1983 for catalysis.[6] The SPO ligands exist in two tautomeric forms and show the an equilibrium between the pentavalent phosphine(V) oxide and the trivalent phosphinous(III) acid (PA) in solution.[7] The SPOs or phosphinito ligands display a stronger cycloisomerization of arenyne.[11] Stephenson *et al.* reported the ruthenium complex **E**, which contains a polydentate ligand composed of one phosphinito and two PA groups (Scheme 1).[12] In addition, very recently Zhang and his co-workers developed a novel secondary phosphine oxide of ruthenium σ-donating ability in their anionic form through oxygen atom compared to phosphinous(III) acid and phosphine ligands.[8] However, this coordination mode has been observed most scarcely with early and late transition metals.[8,9] To the best of our knowledge, only a few ruthenium complexes containing SPO or PA ligands have been reported and their potential applications in catalysis have been studied. For example, [Ru(η^6-arene)(R^{1}R^{2}POH), (**A**: R^1 = R^2 = Me; **B**: R^1 = R^2 = Ph) complexes (Scheme 1) act as catalysts in nitrile hydration.[10] Further, Clavier and co-workers synthesized a series of ruthenium complexes bearing either one SPO ligand (**C**) or two PAs (**D**) and studied their catalytic behaviour for the

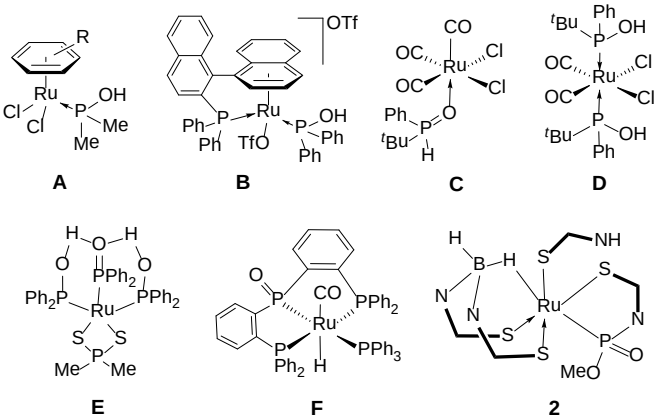

Scheme 1 PA or SPO-based ruthenium complexes

complex (**F**), which shows excellent catalytic activity for the reduction of α,β-unsaturated aldehydes.[13]

The importance of transition metal complexes showing an [M]···H-B interaction (σ or agostic) has been realized in metal-catalyzed B-H activation and hydroboration reactions.[14-16] For example, the activation of B-H bond of H$_3$N·BH$_3$ was facilitated by a highly electrophilic Ru complex, [RuCl(dppe)$_2$]$^-$, via Ru···H-

a. *Department of Chemistry*
Indian Institute of Technology Madras, Chennai 600036, India E-mail: sghosh@iitm.ac.in.

b. *Univ Rennes, CNRS, Institut des Sciences Chimiques de Rennes, UMR 6226, F- 35042 Rennes, France.*

†Electronic Supplementary Information (ESI) available: Spectroscopic and crystallographic data, the coordinates of the calculated geometries using density functional theory (DFT). CCDC 1588902 (**2**), 1588858 (**3**), 1890802 (**4b**), 1588859 (**5a**), 1875698 (**5b**), 1890801 (**6a**), 1824575 (**7a**).
See DOI: 10.1039/x0xx00000x

B interaction.[17] Similarly, activation of monosubstituted boranes RBH_2 or RBH_3Li (alkyl, aryl and NR_2) achieved by Ru complexes $[RuH_2(\eta^2\text{-}H_2)_2(PCy_3)_2]$ or $[Ru(H)Cl(\eta^2\text{-}H_2)(Pcy_3)]$.[15a-b] In this context, the [M]···H-B bonding motifs are reported for both base-stabilized (Shimoi-type)[18] and base-free[19] complexes.

With the objective of synthesizing complexes having [M]··H-B interactions, we recently isolated a series of borate complexes
from the reaction of $[(Cp^*Ru)_2B_3H_9]$ or $[Cp^*MCl_2]_2$ with mbz or $Na[H_2B(mbz)_2]$ (M = Ru, Rh or Ir; Cp* = η^5-C_5Me_5) and studied their reactivity.[20-21] As a result, we explored the reactivity of the sodium salts of $[H_2B(mbz)_2]^-$ further, with different metal precursors, $[(\eta^6\text{-}p\text{-cymene})RuP(OR)_2OR')Cl_2]$, (**1a**: R = R' = Me; **1b**: R = Me, R' = H; **1c**: R = R' = Ph). Herein, we report the synthesis and characterization of novel ruthenium borate complexes that feature secondary phosphine oxide or phosphinate and exhibit two adjacent Ru···H-B interactions of nearly similar nature, respectively. In addition, reactivity studies of one of these complexes with various phosphorus-based ligands leading to the generation of novel coordinated metal-boron complexes are discussed.

Results and discussion

As shown in Scheme 2, room temperature reaction of **1a** or **1b** with two equivalents of $Na[H_2B(mbz)_2]$ (mbz = 2-mercaptobenzothiazolyl) in THF resulted in the formation of $[(L)Ru\{\kappa^3\text{-}H,S,S'\text{-}H_2B(L)_2\}P(O)(OMe)(LH)]$, **2**, $[Ru\{\kappa^3\text{-}H,S,S'\text{-}H_2B(L)_2\}_2]$, **3** and $[(\kappa^2\text{-}N,S\text{-}L)P(OMe)_3Ru\{\kappa^3\text{-}H,S,S'\text{-}H_2B(L)_2\}]$, **4a** (L $C_7H_4NS_2$) in moderate yields. These compounds were separated by preparative thin-layer chromatography, that gave pure
materials for characterisations.

The solid-state structure of **2** was confirmed by X-ray diffraction analysis of a single crystal, obtained from a solution from CH_2Cl_2 at -5 °C and was characterized by mass spectrometry as well as various multinuclear spectroscopic analyses. The ^{1}H NMR spectrum of **2** recorded at 25 °C in $CDCl_3$, displayed a broad signal at δ = -3.40 ppm that corresponds to a bridging proton (B-H_b), and multiplet in the region of 10.98–7.41 ppm, indicating the presence of benzothiolyl groups. The singlet at δ = 152.8 ppm in $^{31}P\{^1H\}$ NMR spectrum, gives an indication that phosphorus is coordinated to the metal centre.[10-13] Furthermore, the $^{11}B\{^1H\}$ NMR spectrum displayed a sharp signal at δ = -4.0 ppm. In addition, the $^{13}C\{^1H\}$ NMR spectrum revealed resonances for the existence of a methyl group and benzothiolyl heterocycles. Mass spectrometry data of **2** showed a molecular peak at *m/z* 858.8385, which corresponds to the composition of $C_{29}H_{23}RuS_8N_4BPO_2$. The infrared (IR) spectrum exhibits the stretching frequencies at 2459 cm^{-1} for B-H_t and 1030 cm^{-1} for the characteristic double bond between phosphorous and oxygen atoms (P=O).

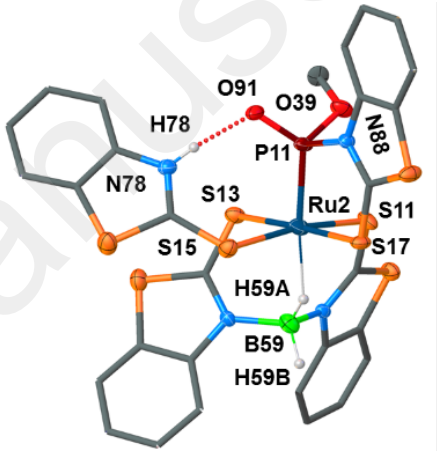

Fig. 1. Molecular structure and labelling diagram for **2** (hydrogen atoms of benzene rings and methyl group are omitted for clarity). Selected bond lengths (Å) and angles (°): Ru2-P11 2.2101(10), Ru2-S11 2.3301(10), Ru2-S15 2.4230(10), Ru2-S17 2.3485(10), Ru2-H59A 1.90(4), B59-H59A 1.14(5), B59-H59B 1.13(4), P11-O91 1.504(3), P11-O39 1.616(3); P11-N88 1.803(3), Ru2-P11-N88 105.30(11), P11-Ru2-S11 93.05(4), H59A-B59-H59B 101(3).

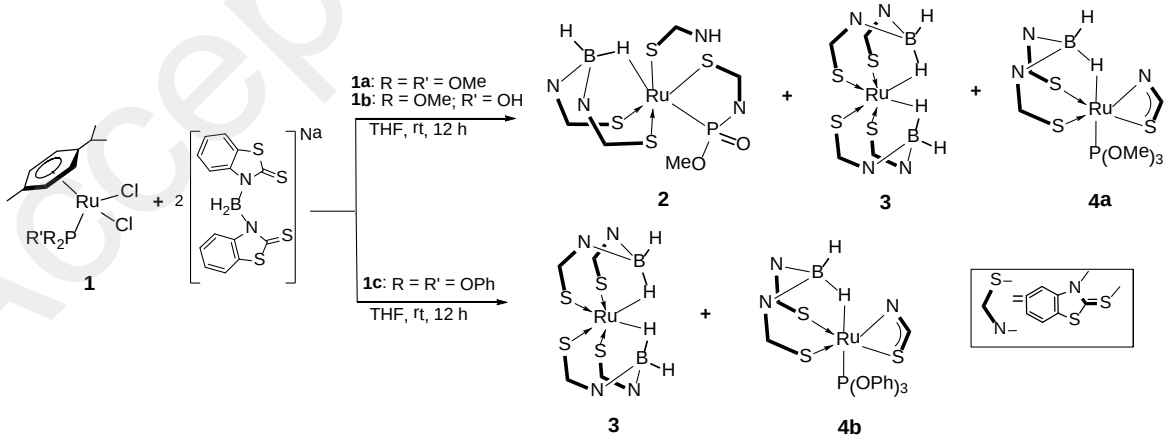

Scheme 2 Synthesis of ruthenium complexes supported by benzothiazolyl heterocycles **2-4**.

Compound **2** contains two independent molecules in the unit cell. The molecular structure adopts a unique coordination fashion between the metal and ligands, which differs from reported metal-SPO complexes[10-13] (Fig. 1). Interestingly, the

phosphorus atom of the chiral secondary phosphine oxide and sulphur atom of the benzothiolyl group are bonded to ruthenium in the octahedral coordination core of **2** and form a five-membered (RuSONP) ring (Fig. 1). The oxygen atom of P=O bond has hydrogen bond interaction with H atom of pendanted benzothiolyl moiety. The bond length between P11 and O91 (1.504(3) Å) indicates a double bond, characteristic for metal-SPO complexes.[9a,10-13] This bond distance suggests that the phosphorus atom is bonded with the ruthenium centre through σ-bond and the P=O bond (P^{V}) formed by oxidation as it is major unit in equilibrium with (P^{III}) tautomer.[7,11] Notably, the Ru2-P11 bond distance (2.2101(10) Å) is shorter than corresponding distances in other metal-SPO complexes,[10-13,22] maybe due to the involvement of Ru and P in the formation of five membered ring. In addition, the Ru2-S13 distance (2.4031(10) Å) is elongated compared to that of Ru2-S11 bond (2.3301(10) Å) and Ru2-H59 Å bond distance of 1.90(4)Å, are in the range of values measured in reported ruthenium borate complexes.[20,21]

In order to have insight into the structure and bonding of **2**, density functional theory (DFT) computations were carried out. The geometrical parameters of the optimised ground-state structure at PBE0/def2-TZVP level of theory are in a good agreement with the corresponding experimental ones (Table S1†). The calculated P=O stretching frequency, 1055 cm^{-1}, is in accordance with the experimental value, 1030 cm^{-1}. Further, both the ^{11}B and ^{1}H chemical shifts were computed by the well known GIAOs (gauge-including atomic orbitals) method and compared with observed values (Table S3†). The natural population analysis (NPA), shown in Table S2, suggests that the

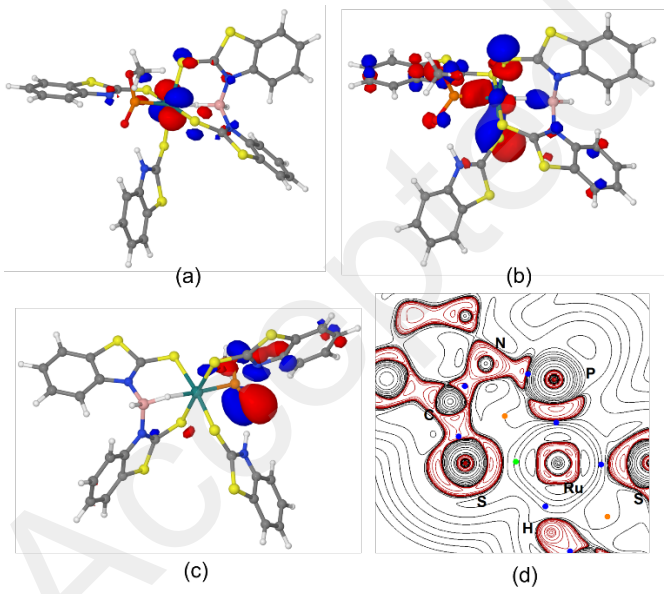

Fig. 2. HOMO (a), HOMO-7 (b) and HOMO-16 (c) of **2** respectively (isovalue: ±0.05 $[e/bohr^3]^{1/2}$); contour plot of Laplacian of the electron density, $\nabla^2\rho(r)$ (d) with negative contours shown as red lines and positive contours shown as black lines for **2** (blue and yellow dots indicate *bcps* and *rcps,* respectively).

P atom has more positive charge, indicating that less electron density surrounds it, which is consistent with more downfield chemical shift in $^{31}P\{^{1}H\}$ NMR spectrum. Analysis of molecular orbitals reveals that the HOMO of **2** mainly composed of ruthenium d_{xy}-character with small p_x-character of sulphur of the benzothiazolyl ligands (Fig. 2a), while the LUMO had mainly on ligands (Fig. S49). The HOMO-7 and HOMO-16 in **2** involves Ru-P and P=O bonding interactions respectively (Fig. 2b,c).

In addition, the coordination of phosphinate and B-H units with Ru metal in **2** are supported by topological and natural bond orbital (NBO) analyses. The topological analysis shows the presence of bond critical points (bcps) for Ru2-P11 [ρ (0.120 au) and $\nabla^2\rho(r)$ (0.175 au)] and Ru2-S15 [ρ (0.213 au) and $\nabla^2\rho(r)$ (0.420 au)] bonds (Fig. 2d, Table S4). The ellipticity of the electron density at bcps of R-H and H-B bonds indicates Ru-H-B interaction (Fig. S49, Table S4). Furthermore, the inspection of an NBO analysis provided relatively high WBI (Wiberg bond index) value of 1.093 for the P-O bond, which is consistent with a double bond character. Other bonding interactions between the atoms for specific bonds, for example Ru-P, Ru-S, P-O, P-N and Ru-H-B, bonds are shown in Fig. S50.

Compound **3** was isolated as yellow crystals and was characterized by IR, ^{1}H, $^{11}B\{^{1}H\}$, $^{13}C\{^{1}H\}$ NMR and mass spectrometry (Fig. S6-S8 and S41†). The mass spectrum of **3** showed a molecular ion peak at *m/z* 792.8675 ($[M+H]^+$). The $^{11}B\{^{1}H\}$ NMR spectrum shows a broad signal at δ = -4.8 ppm and the ^{1}H NMR spectrum shows a upfield chemical shift at δ = -11.94 ppm, consistent with the metal-coordinated proton. The spectroscopic data combined with the mass spectrometric data were not adequate to predict the identity of **3**. A clear explanation eluded us until a solid-state X-ray structure analysis of **3** was carried out.

The molecular structure of **3**, shown in Fig. 3a, can be seen as [Ru{κ^3-H,S,S′-$H_2B(L)_2$}$_2$] (L = $C_7H_4NS_2$). The Ru atom in **3** is in a

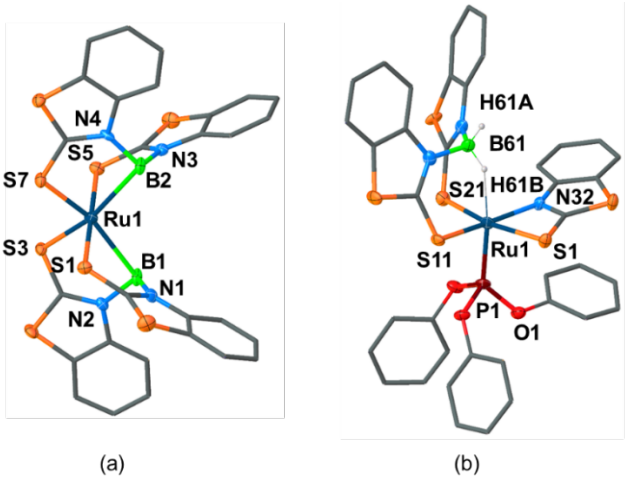

Fig. 3. Molecular structures and labelling diagram for **3** and **4b** (hydrogen atoms of benzene rings are omitted for clarity). Selected bond lengths (Å) and angles (°). (a): Ru1-B1 2.644(11), Ru1-B2 2.631(10), Ru1-S1 2.379(2), Ru1-S3 2.300(2), Ru1-S5 2.369(2), Ru1-S7 2.313(2), B1-N1 1.577(12), B2-N3 1.568(12); S3-Ru1-S7 88.70(8), S5-Ru1-S7 89.99(9), B1-Ru1-B2 107.0(3), N2-B1-Ru1 98.2(5), N3-B2-Ru1 97.7(5); (b): Ru1-H61B 1.938, Ru1-S1 2.4495(17), Ru1-S11 2.3148(17), Ru1-S21 2.3553(17), Ru1-N32 2.130(5), Ru1-P1 2.1833(19), P1-O1 1.603(6), B61-H61B 0.9700, N32-Ru1-P1 100.04(16), P1-Ru1-S1 91.76(7), H61A-B61-H61B 107.70.

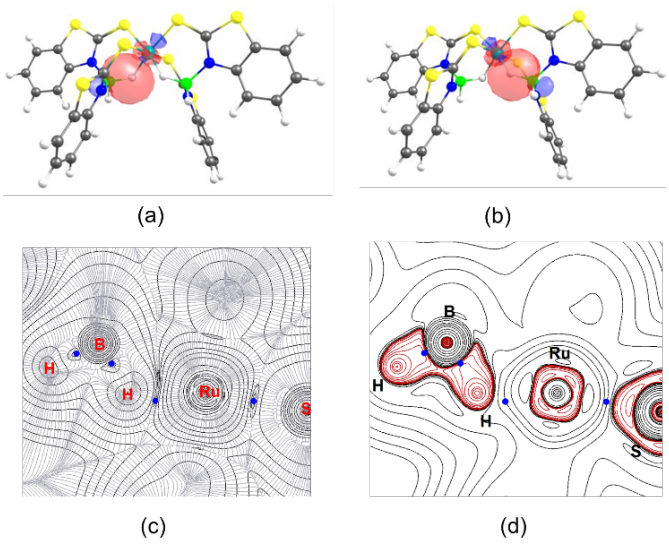

Fig. 4. (a) and (b) Natural bond orbitals associated with Ru-H-B interactions in **3**; (c) contour plot of electron density overlaid with gradient in grey colour and bond critical points as blue points; (d) contour plot of the Laplacian of the electron density with negative contours shown as red lines and positive contours shown as black lines for **3** in one of Ru-H-B plane.

distorted octahedral geometry surrounded by tridentate $[H_2B(mbz)_2]^-$ groups in (κ^3-H,S,S') coordination mode. The presence of B-H_b and B-H_t hydrogen atoms in **3** were confirmed by ^{1}H-^{11}B HSQC NMR spectroscopy (Fig. S9). The Ru-B distances of 2.644(11) Å and 2.631(10) Å are shorter as compared to those in [Cp*Ru{κ^3-H,S,S'-$H_2B(L)_2$}] (2.753(1) Å)[20a] and [(cod)ClRu{κ^3-H,S,S'-$H_2B(L)_2$}] (2.697(4) Å)[20d] (L = $C_7H_4NS_2$). However, they are considerably longer than the Ru-B distance observed in [RuH_2{η^2-HB:η^2-HC-HB(N^{i}Pr$_2$)$CH_2C_6H_4PPh_2$}(PCy_3)] (2.173(3) Å)[23] as well as in ruthenaborane clusters.[24] The two S,B,S-donor sets in **3** are aligned in *fac*-arrangements that minimizes the steric repulsion between them.

Furthermore, to study the bonding nature of the Ru-H-B interaction, calculations were performed on **3**. The optimised structure fits well with the X-ray crystal structure (Table S1†). The energy gap between the HOMO (highest occupied molecular orbital) and LUMO (lowest occupied molecular orbital) for **3** is 1.88 eV (Table S2†). NBO studies suggest that there are two sets of weak Ru···H-B interactions in the molecule (Fig. 4a-b). WBI for the Ru-H bond (0.191) is notably smaller compared to that of the B-H_b bond (0.657). This suggests a weak Ru-H interaction (Table S1†). In line with the NBO calculations, the topology of the electron density for **3** shows that the B-H moieties that interact with the metal centre, have similar electron densities and Laplacian of the electron densities at Ru-H bond critical points (bcps) (Table S4). This indicates the presence of equivalent interactions in the two Ru-H-B planes for **3** (Fig. 4c-d).

In parallel to the formation of **2** and **3**, reaction of **1a** with $Na[H_2B(mbz)_2]$ also yielded the novel ruthenium borate complex [(κ^2-*N,S*-L)$P(OMe)_3Ru${κ^3-H,S,S'-$H_2B(L)_2$}], **4a**, by ruthenium-induced B-N bond cleavage of the $[H_2B(mbz)_2]^-$ ligands.[25] Unfortunately, **4** was not yielded from **1b** under same or different conditions, this may be due to the fact that $P(OMe)_2OH$ gets easily oxidized and converted to **2**. The $^{31}P\{^1H\}$ NMR spectrum of **4a** shows a single peak at δ = 144.2 ppm. The $^{11}B\{^1H\}$ NMR spectrum shows a broad peak at δ = -4.0 ppm. Besides the presence of protons due to mbz moieties, the ^{1}H NMR spectrum exhibits one upfield chemical shift at δ = -2.32 ppm corresponding to Ru–*H*–B proton and δ = 4.78 to 3.63 ppm for B-H_t units. Further, the mass spectrum of **4a** displayed a molecular ion peak at *m/z* 737.8978, suggesting the molecular formulation of $C_{24}H_{24}RuS_6N_3BPO_3$.

Under the similar reaction conditions, the reaction of [(η^6-*p*-cymene)$RuCl_2P(OPh)_3$], **1c**, with two equivalents of same borate ligand yielded [Ru{κ^3-H,S,S'-$H_2B(L)_2$}$_2$], **3**, and [(κ^2-*N,S*-L)$P(OPh)_3Ru${κ^3-H,S,S'-$H_2B(L)_2$}], **4b**, (L = $C_7H_4NS_2$) in yellow and red solids (Scheme 2). Based on all the spectroscopic data combined with mass spectrometric studies, it is clear that **4b** is analogous to **4a**. As shown in Fig. 3b, the molecular structure of **4b**, in which the Ru atom is in a distorted octahedral environment with a $P(OPh)_3$ ligand and one σ-B-H interaction. The Ru···H-B distance of 1.975 Å in **4b** is considerably longer as compared to **2** (1.90(4) Å), as well as in reported borate complexes, such as for example, [Cp*Ru{κ^3-H,S,S'-$H_2B(L)_2$}] (1.830(3) Å)[20a] and [(cod)Ru(L){κ^3-H,S,S'-$H_2B(L)_2$}] (1.755(3) Å)[20d] (L = $C_7H_4NS_2$). Similarly, the Ru···B distance of 2.817 Å in **3a** is significantly longer as compared to that in **2** (2.784 Å), and **3** (2.644(11) Å).

Phosphines or phosphites are generally considered as good donor ligands.[1,26] We then envisaged that a ready accessibility of these ligands might show interesting reactivity towards **3**. Thus, we performed the reaction of **3** with one equivalent of $P(OR)_3$ (R = Me or Ph) at 60 °C in toluene. This resulted in the formation of the phosphite-incorporated borate complexes [$(OR)_3PRu${κ^2-S,S'-H_2BL_2}{κ^3-H,S,S'-H_2BL_2}], (**5a**: R = Me, **5b**: R = Ph; L = $C_7H_4NS_2$) as brown crystalline solids (Scheme 3). The $^{31}P\{^1H\}$ NMR spectrum for both complexes provides a chemical shift in the expected region for the four coordinate phosphorus atom[27] (δ = 136.0 ppm for **5a** and δ = 116.6 ppm for **5b**). This suggests the incorporation of the phosphite unit. Along with aromatic features, the B-H_b and B-H_t protons in the region of -4.44 - -4.13 ppm and 4.38-4.23 ppm respectively are observed in ^{1}H NMR spectroscopy. Further, the presence of borate units are suggested by sharp signals at δ = -3.1 and -6.3 ppm for **5a** and δ = -3.3 and -6.8 ppm for **5b** in the $^{11}B\{^1H\}$ NMR spectra. A molecular ion peak at *m/z* 916.9013 and 1102.9442 in the mass

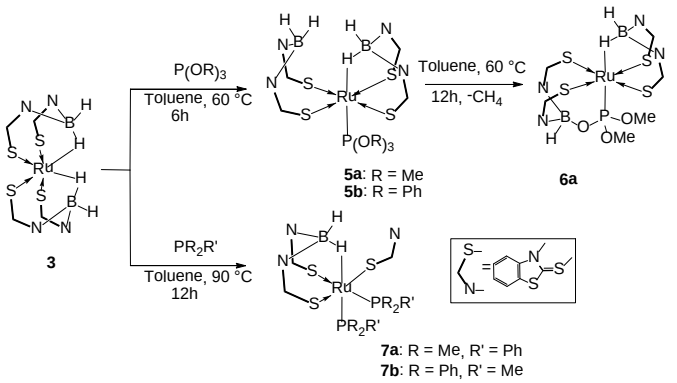

Scheme 3 Reactivity of **3** with various phosphorus based ligands.

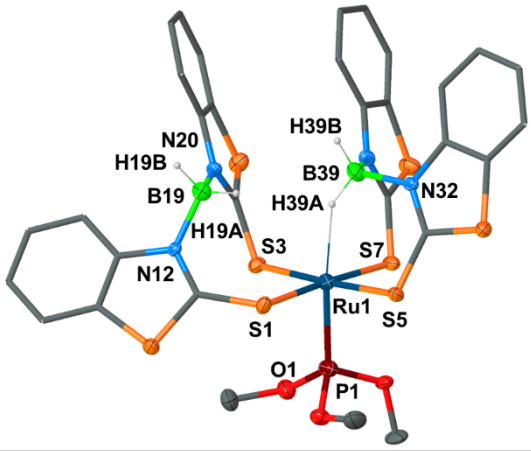

(a)

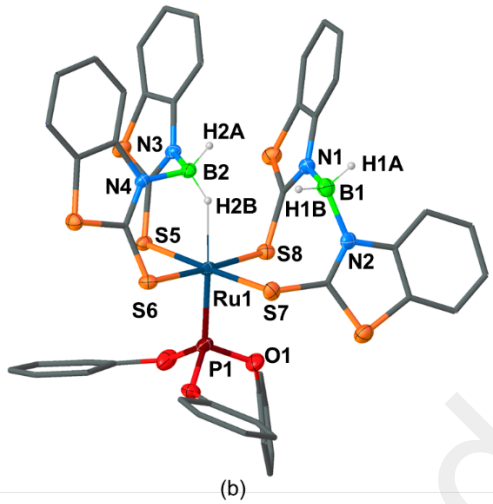

(b)

Fig. 5. Molecular structure and labelling diagram for **5a** (a) and **5b** (b) (hydrogen atoms of benzene rings are omitted for clarity). Selected bond lengths (Å) and angles (°) (**5a**): Ru1-H39A 1.973, Ru1-S1 2.4186(16), Ru1-S5 2.3276(18), Ru1-S7 2.3672(16), Ru1-P1 2.2081(15), B39-H39A 0.9900; S1-Ru1-S3 95.91(6), S5-Ru1-S7 90.32(6), P1-Ru1-S1 92.74(6), H39A-B39-H39B 108.0; (**5b**) Ru1-B2 2.791, Ru1-H2B 1.938, B1-H1A 0.9700, B1-H1B 0.9700, B2-H2B 0.9700, Ru1-P1 2.1832(16), P1-O1 1.604(4), Ru1-S5 2.3625(14), Ru1-S8 2.4254(17); S5-Ru1-S6 89.33(6), S7-Ru1-S8 9 94.45(6), P1-Ru1-S6 93.48(6), H1A-B39-H1B 108.3, H2A-B2-H2B 107.9.

spectra confirmed the formulation of **5a** and **5b** respectively. Their solid-state X-ray structures clearly shows that one unit of $[H_2B(mbz)_2]$ is bonded to Ru through a (κ^3-H,S,S') coordination mode and that the other one is connected *via* a (κ^2-S,S') mode forming an eight-membered ring (Fig. 5).‡ The Ru-S bond lengths are rather similar in both cases, but the Ru-P and Ru-B bond distances of 2.2081(15) Å and 2.828 Å respectively in **5a**, are longer than the corresponding ones in **5b** (Ru-P 2.1832(16) Å; Ru-B 2.791 Å) and **3** (Ru-B 2.644(11) Å.

Interestingly, upon heating compound **5a**, it readily changes into the novel air stable red compound $[(OMe)_2OPRu\{\kappa^2\text{-S,S'-HB(L)}_2\}\{\kappa^3\text{-H,S,S'-H}_2\text{B(L)}_2\}]$, **6a** (L = $C_7H_4NS_2$) in quantitative yield (Scheme 3). The ^{1}H NMR spectrum of **6a** shows two distinct hydrogen environments, one at δ = -3.15 and and the other at 3.71, 3.69 ppm, which are assigned to the terminal and bridging B-H protons, respectively. The $^{31}P\{^1H\}$ NMR spectrum at room temperature reveals a single resonance at δ = 132.3 ppm, up-field shifted relative to that of the parent compound **5a** (δ = 136. 0 ppm). Compound **6a** also exhibits two sharp chemical shifts in the $^{11}B\{^1H\}$ NMR spectrum at δ = 0.1, -4.6 ppm, shifted downfield compared those of **5a** (δ = -3.1, -6.3 ppm). In addition, the $^{13}C\{^1H\}$ NMR spectrum suggests the presence of methoxy groups and benzothiolyl heterocycles. Further, the existence of a bridging and terminal B-H protons are consistent with IR spectroscopy.

An unambiguous determination eluded us until a solid-state X-ray structure analysis of **6a** was performed. The crystalline solid of **6a** was found to consist of two independent molecules within the asymmetric unit. The molecular structure of **6a** is shown in Fig. 6, along with selected bond parameters. The key feature of **6a** is the formation of P-O and O-B bonds by release of methane maybe from the methoxy group of the phosphite and the terminal hydrogen of the borate ligand. The ruthenium centre is also bonded to the anionic $[BH_2(mbz)_2]$ and $[BH(mbz)_2]$ ligands, which are linked through the thione donors and BH units (Fig. 6). It also contains the phosphite group and then the coordination around the ruthenium centre is a distorted octahedral geometry. The phosphorous-oxygen and boron-oxygen bond distances are 1.568(6) Å and 1.450(12) Å respectively, consistent with other structurally characterized complexes having P-O and B-O moieties.[28,29] The Ru1-P1 bond length of 2.180(3) Å is shorter than in the parent compound **5a** (2.2081(15) Å). The Ru1-B2 (2.803 Å), Ru1-H5X (1.88(8) Å) and B2-H5X (1.15(8) Å) distances are matches well with the corresponding ones measured in other related complexes.[20]

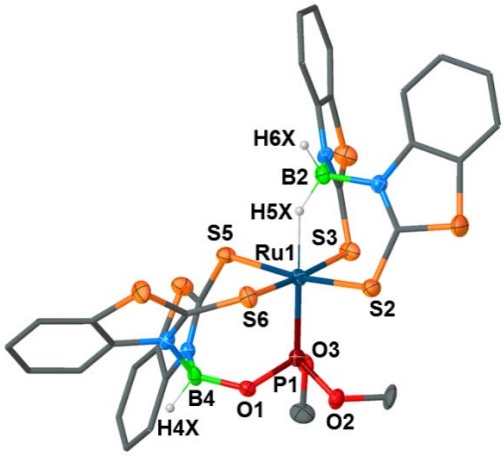

Fig. 6. Molecular structure and labelling diagram for **6a** (hydrogen atoms of benzene rings and methyl groups are omitted for clarity). Selected bond lengths (Å) and angles (°): Ru1-P1 2.180(3), Ru1-S2 2.343(3), Ru1-S6 2.364(3), Ru1-H5X 1.88(8), P1-O1 1.568(6), P1-O2 1.618(7), B2-H5X 1.15(8), B2-H6X 1.13(10), B4-H4X 1.06(6), B4-O1 1.450(12); Ru1-P1-O1 116.4(3), B4-O1-P1 127.9(6), O1-B4-H4X 112(4), H5X-B2-H6X 105(6).

The computed HOMO-LUMO energy gap of **6a** is greater compared to that computed for **5a** and **5b** (Table S2). The HOMO is mainly located on the ruthenium centre with a small

contribution from the metal-coordinated sulphur atoms. On the other hand, the LUMO is primarily on one of the benzothiazolyl moieties and the Ru centre (Fig. 7a-b). From an NBO analysis, the Wiberg bond indices (WBI) of Ru-P, P-O and B-O bonds are

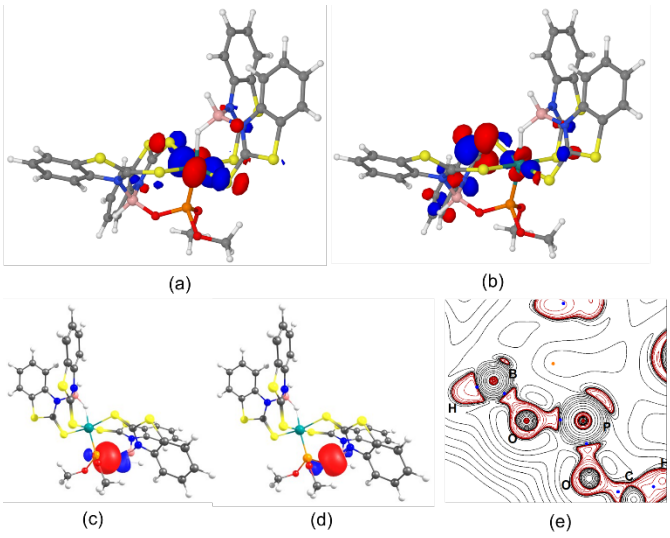

Fig. 7. HOMO (a) and LUMO (b) of **6a** (isovalue: ±0.05 [e/bohr^3]$^{1/2}$); bonding interaction between P-O bond (c) and B-O bond (d) as obtained from NBO analysis; contour plot of Laplacian of the electron density, $\nabla^2\rho(r)$ (e) with negative contours shown as red lines and positive contours shown as black lines for **6** (blue dots indicate *bcps*).

0.760, 0.778 and 0.766, respectively, indicating strong coordinative interaction, which matches well with the crystal data (Fig 7c-d and S52, Table S1). The topological analysis of the electron density shows that bond critical points (bcps) between Ru-P, P-O, B-O, R-H and H-B bonds (Fig. 7e and S51, Table S4).

We were interested in the structural changes in the coordination sphere of the ruthenium centre upon reaction with other phosphine ligands. As a result, we carried out the reaction of **3** with PR_2R' (R = Me or Ph; R' = Ph or Me) at 90 ˚C, that afforded generation of [Ru({κ^3-H,S,S'-$H_2B(L_2)$}$(PR_2R')_2$(L)], (**7a**: R = Me, R' = Ph; **7b**: R = Ph; R' = Me; L = $C_7H_4NS_2$), respectively, in moderate yields. Interestingly, the $^{31}P\{^1H\}$ NMR spectra of **7a** and **7b** displayed doublet of doublet in the range of δ = 12.9-27.1 ppm, thereby suggesting that two phosphorus atoms are coordinated to the metal centre. The less positive

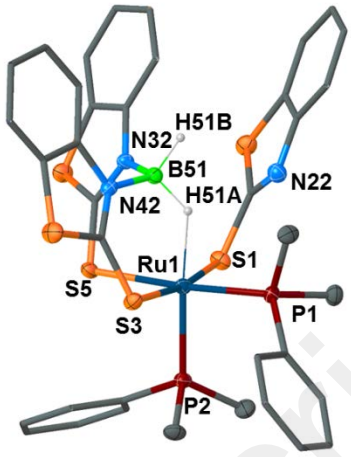

Fig. 8. Molecular structures and labelling diagram for **7a** (hydrogen atoms of benzene rings and methyl groups are omitted for clarity). Selected bond lengths (Å) and angles (°): Ru1-H51A 1.84(2), Ru1-S1 2.4097(6), Ru1-S3 2.3578(6), Ru1-P1 2.3034(6), Ru1-P2 2.2719(6), B51-H51A 1.15(2), B51-H51B 1.13(2); P2-Ru1-P1 91.61(2), P2-Ru1-S3 94.06(2), S3-Ru1-H51A 86.5(7), S1-Ru1-H51A 88.7(7), S5-Ru1-H51A 91.7(7).

NPA charges of phosphorous atom suggest more electron density around them, consistent with the more up-field shift in their $^{31}P\{^1H\}$ NMR compared that of **2**-**6** (Table S2). The $^{11}B\{^1H\}$ NMR spectra showed a broad resonance at δ = -2.9 ppm for **7a** and –2.1 ppm for **7b**, respectively. The ^1H NMR spectra reveal a broad signal in the region of δ = -6.93- –7.63 ppm for B-H_b protons and a multiplet in the range of 7.82–6.80 ppm, indicating the presence of benzothiolyl groups in both compounds. Further, $^{13}C\{^1H\}$ NMR spectra confirm the presence of methyl and benzothiolyl heterocycles and ESI mass spectra in positive mode displyed a molecular ion peak at *m/z* 889.9925 and 1014.0246 for **7a** and **7b**, respectively.

The solid-state structure of **7a** could be unambiguously determined by means of single crystal X-ray diffraction analysis. To our surprise, it indicates that two units of phosphine ligands are incorporated in its coordination sphere, contrary to only one
in the cases of **2** and **5**. The ruthenium atom in **7a** adopts an octahedral geometry with two phosphine units, both positioned in *cis*-arrangement (Fig. 8). The ruthenium centre is also connected to the $[BH_2(mbz)_2]$ ligand *via* (κ^3-H,S,S') and one benzothiozolyl heterocycle unit through a η^1-coordination mode. The Ru-P bond lengths in **7a** (2.3034(6) Å and 2.2719(6) Å) are elongated with respect to those in **2** (2.2053(10) Å) and **5** (2.2081(15) Å). The Ru1-H51A (1.84(2) Å) and B51-H51A (1.15(2) Å) bond distances are comparable with the corresponding observed distances in **3** and other reported ruthenium borate complexes.[20]

Conclusions

In summary, the synthesis of ruthenium borate complexes featuring a secondary phosphine oxide moiety has been successfully achieved with simple phosphine ligands. Among them, one eighteen-electron bis(mercapto-benzothiazolyl)-borate complex of ruthenium with two adjacent Ru···H-B

interactions has been synthesized. Further, utilization of more basic phosphines in metal precursors led to the formation of phosphorous incorporated compounds. While a very few number of borate complexes having dual Ru···H-B interactions are known, their reactivity has not been further explored at length. Here, we explored the chemistry of a ruthenium bis(borate) complex, with a set of phosphorus-based ligands, that clearly demonstrate the flexible nature of [M]···H-B interactions and revealed a diverse reactivity pattern by incorporating phosphite and phosphine units in the coordination sphere of ruthenium.

Experimental

General procedures and instrumentation

All manipulations were conducted under standard Schlenk line and glove box techniques at inert atmosphere of dry argon. Compounds $[(\eta^6\text{-}p\text{-cymene})Ru(PR_2R')Cl_2]$[27a,30] (**1a**: R = R′ = OMe; **1b**: R = OMe, R′ = OH; **1c**: R = R′ = OPh) and $Na[H_2B(mbz)_2]$[31] (mbz = 2-mercaptobenzothiazolyl) were prepared according to the literature procedures. Toluene, Hexane and THF were distilled (from Na/benzo-phenoneketyl) when required and CH_2Cl_2 was dried over calcium hydride. $CDCl_3$ was degassed by three freeze-thaw cycles, dried over calcium hydride for 12 h, and kept in a Young's ampoule over 4 Å molecular sieves under Argon. The ^1H, $^{11}B\{^1H\}$, $^{13}C\{^1H\}$, $^{31}P\{^1H\}$ and HSQC NMR spectra were recorded on a Bruker 400 and 500 MHz instruments. The external reference for the $^{11}B\{^1H\}$ NMR spectroscopy, $[Bu_4N][(B_3H_8)]$ was synthesized according to the literature method.[32] Residual solvent protons were used as reference (δ, ppm, benzene-d_6, 7.16, $CDCl_3$, 7.26), while a sealed tube containing $[Bu_4N][(B_3H_8)]$ in benzene-d_6 (δ_B, ppm, -30.07) was used as an external reference for $^{11}B\{^1H\}$ NMR spectra. ^1H decoupled $^{11}B\{^1H\}$ spectra of all compounds were processed with a backward linear prediction algorithm to remove the broad $^{11}B\{^1H\}$ background signal of the NMR tube.[33] Mass spectra were carried out using Bruker MicroTOF-II mass spectrometer and Qtof Micro YA263 HRMS instrument in ESI ionization mode. The FT-IR spectra were recorded using a Jasco FT/IR-4100 spectrometer.

Synthesis of 2-4

$[(\eta^6\text{-}p\text{-cymene})RuCl_2P(OMe)_3]$, **1a** (0.120 g, 0.279 mmol) and $Na[H_2B(mbz)_2]$ (mbz = 2-mercaptobenzothiazolyl) (0.205 g, 0.558 mmol) were taken in a flamed dried Schlenk flask and placed at room temperature. Dry THF (15 mL) was slowly added to these solids under stirring condition. Upon addition of THF, a reddish orange solution formed, which was stirred at same temperature for 12 h. The solvent was removed *in-vacuo* and the residue was dissolved in CH_2Cl_2 (15 mL)/Hexane (5 mL), filtered using Celite. The solvent was removed and the residue was subjected to chromatographic workup using silica-gel TLC plates. Elution with a CH_2Cl_2/hexane (70:30 v/v) mixture yielded an orange **2** (0.060 g, 25%), yellow **3** (0.050g, 22%), and red **4a** (0.080 g, 34%).

Under same reaction conditions, treatment of $[(\eta^6\text{-p-cymene})RuCl_2P(OMe)_2OH]$, **1b** (0.120 g, 0.289 mmol) with $Na[H_2B(mbz)_2]$ (0.212 g, 0.578 mmol) yielded an orange **2** (0.076 g, 30%) and yellow **3** (0.080 g, 35%).

Red compound **4b** (0.046 g, 25%) and yellow compound **3** (0.076 g, 50%) were isolated from the reaction of $[(\eta^6\text{-}p\text{-cymene})RuCl_2P(OPh)_3]$, **1c** (0.120 g, 0.194 mmol) with $Na[H_2B(mbz)_2]$ (0.212 g, 0.388 mmol) under similar reaction conditions of **4a**.

2: MS (ESI^+): *m/z* calculated for $C_{29}H_{23}RuS_8N_4BPO_2$ $[M+H]^+$: 858.8460, found 858.8385; $^{11}B\{^1H\}$ NMR (160 MHz, $CDCl_3$, 22°C): δ = -4.0; ^1H NMR (500 MHz, $CDCl_3$, 22°C): δ = 10.98 (s, 1H), 8.39 (d, *J* = 8.4 Hz, $1H_{Ar(mbz)}$), 7.87 (d, *J* = 8.6 Hz, $1H_{Ar(mbz)}$), 7.80 (d, *J* = 8.5 Hz, $1H_{Ar(mbz)}$), 7.69–7.64 (m, $1H_{Ar(mbz)}$), 7.48–7.43 (m, $4H_{Ar(mbz)}$), 7.41–7.32 (m, $5H_{Ar(mbz)}$), 7.29 (dd, *J* = 7.8, 6.3 Hz, $6H_{Ar}$), 7.25–7.19 (m, $2H_{Ar(mbz)}$), 4.96 (br, 1H, B-H_t), 3.97 (d, *J* = 11.6 Hz, 3H P(OCH_3), -3.40 (s, br, 1H, Ru-*H*-B); $^{13}C\{^1H\}$ NMR (125 MHz, $CDCl_3$, 22°C): δ = 53.6, 112.1, 114.8, 116.4, 116.7, 117.3, 121.3, 124.3, 124.4, 124.6, 124.9, 126.6, 126.7, 127.3, 130.2, 140.2, 142.7, 191.1, 191.2 (C=S); $^{31}P\{^1H\}$ NMR (121 MHz, $CDCl_3$, 22°C): δ = 152.8; IR (CH_2Cl_2, cm^{-1}): $\tilde{\nu}$ = 2459 (B-H_t), 2103 (B-H_b), 1030 (P=O).

3: MS (ESI^+): *m/z* calculated for $C_{28}H_{21}RuS_8N_4B_2$ $[M+H]^+$: 792.8761, found 792.8675; $^{11}B\{^1H\}$ NMR (160 MHz, $CDCl_3$, 22°C): δ = -4.8; ^1H NMR (500 MHz, $CDCl_3$, 22°C): δ = 7.92 (d, *J* = 8.1 Hz, $1H_{Ar(mbz)}$), 7.79–7.69 (m, $4H_{Ar(mbz)}$), 7.47–7.41 (m, $2H_{Ar(mbz)}$), 7.40–7.31 (m, $4H_{Ar(mbz)}$), 7.31–7.26 (m, $2H_{Ar(mbz)}$), 7.24 (d, *J* = 1.4 Hz, $1H_{Ar(mbz)}$), 7.21–7.15 (m, $2H_{Ar(mbz)}$), 4.59 (s, 2H, B-H_t), -11.94 (s, br, 2H, Ru-*H*-B); $^{13}C\{^1H\}$ NMR (125 MHz, $CDCl_3$, 22°C): δ = 116.2, 121.2, 121.5, 122.0, 124.1, 124.2, 124.7, 126.3, 126.4 (C=C), 133.1, 145.2 (C=N), 198.8 (C=S), 199.7 (C=S); IR (CH_2Cl_2, cm^{-1}): $\tilde{\nu}$ = 2456 (B-H_t), 2060 (B-H_b).

4a: MS (ESI^+): *m/z* calculated for $C_{24}H_{24}RuS_6N_3BPO_3$ $[M+H]^+$: 737.9016, found 737.8978; $^{11}B\{^1H\}$ NMR (160 MHz, $CDCl_3$, 22°C): δ = -4.0; ^1H NMR (500 MHz, $CDCl_3$, 22°C): δ = 7.85 (d, *J* = 8.4 Hz, $1H_{Ar(mbz)}$), 7.74 (d, *J* = 8.3 Hz, $1H_{Ar(mbz)}$), 7.64 (d, *J* = 8.1 Hz, $1H_{Ar(mbz)}$), 7.52 (d, *J* = 7.8, 1.2 Hz, $1H_{Ar(mbz)}$), 7.39–7.33 (m, $2H_{Ar(mbz)}$), 7.31–7.27 (m, $1H_{Ar(mbz)}$), 7.22 (td, *J* = 7.8, 1.4 Hz, $1H_{Ar(mbz)}$), 7.19–7.12 (m, $3H_{Ar(mbz)}$), 7.09–7.02 (m, $1H_{Ar(mbz)}$), 4.78 (s, 1H, B-H_t), 3.63 (d, *J* = 11.1 Hz, 9H), -2.32 (s, br, 1H, Ru-*H*-B);$^{13}C\{^1H\}$ NMR (125 MHz, $CDCl_3$, 22°C): δ = 52.7 (OMe), 116.3, 116.6, 121.0, 121.1, 122.6, 124.1, 124.3, 126.0, 126.3, 145.6 (C=N), 182.8 (C=S), 197.0 (C=S); $^{31}P\{^1H\}$ NMR (121 MHz, $CDCl_3$, 22°C): δ = 144.2 ; IR (CH_2Cl_2, cm^{-1}): $\tilde{\nu}$ = 2436 (B-H_t), 2138 (B-H_b).

4b: MS (ESI^+): *m/z* calculated for $C_{39}H_{30}RuS_6N_3BO_3P$ $[M+H]^+$: 923.9485, found 923.9404; $^{11}B\{^1H\}$ NMR (160 MHz, $CDCl_3$, 22°C): δ = -3.7; ^1H NMR (400 MHz, $CDCl_3$, 22°C): δ = 7.78 (d, *J* = 8.4 Hz, $1H_{Ar(mbz)}$), 7.58–7.50 (m, $1H_{Ar(mbz)}$), 7.39–7.33 (m, $2H_{Ar(mbz)}$), 7.19–7.13 (m, $10H_{Ar}$), 7.09 (dd, *J* = 8.8, 7.0 Hz, $7H_{Ar(mbz)}$), 6.95–6.86 (m, $6H_{Ar}$), 4.72 (s, 1H, B-H_t), -2.44 (s, br, 1H, Ru-*H*-B); $^{13}C\{^1H\}$ NMR (125 MHz, $CDCl_3$, 22°C): δ = 115.9, 116.5, 119.0, 120.3, 121.1, 122.1, 122.9, 123.9, 124.2, 125.2, 129.1, 134.3, 137.2, 140.0, 149.9, 151.9, 154.9, 192.51 (C=S);

$^{31}P\{^1H\}$ NMR (121 MHz, $CDCl_3$, 22°C): δ = 123.8 ; IR (CH_2Cl_2, cm^{-1}): $\tilde{\nu}$ = 2468 (B-H_t), 2149 (B-H_b).

Synthesis of 5a-b

In a flame dried Schlenk tube, a yellow solution of **2** (0.050 g, 0.063 mmol) and $P(OMe)_3$ (0.07 mL, 0.063 mmol) in toluene (15 mL) was thermalized for 12 h at 60 °C temperature. The volatile components were removed under vacuum and the remaining residue was extracted into CH_2Cl_2/hexane passed through Celite. After removal of solvent, the residue was subjected to chromatographic work up using preparative TLC. Elution with a hexane/CH_2Cl_2 (20:80 v/v) mixture yielded brown **4** (0.020 g, 34%).

Under same reaction conditions, treatment of [Ru{κ^3-H,S,S'-$H_2B(L)_2\}_2$], **3** (0.050 g, 0.063 mmol) with $P(OPh_3)_3$ (0.16 mL, 0.063 mmol) yielded an brown **5b** (0.026 g, 41%).

Although we have tried different conditions, we were unable to isolate **6b** from **5b** or **3**. This may be due to the presence of O-Ph bond that is stronger in $P(OPh)_3$ as compared to O-CH_3 bond in $P(OMe)_3$.

5a: MS (ESI^+): *m/z* calculated for $C_{31}H_{30}RuS_8N_4B_2PO_3$ $[M+H]^+$: 916.9050, found 916.9013; $^{11}B\{^1H\}$ NMR (160 MHz, $CDCl_3$, 22 °C): δ = -3.1 (br, B1), -6.3 (br, B2); ^1H NMR (500 MHz, $CDCl_3$, 22 °C): δ = 7.98 (d, *J* = 8.4 Hz, $1H_{Ar(mbz)}$), 7.32 (d, *J* = 8.5 Hz, $4H_{Ar(mbz)}$), 7.24 (d, *J* = 7.5 Hz, $3H_{Ar(mbz)}$), 7.11 (t, *J* = 7.5 Hz, $5H_{Ar(mbz)}$), 7.05 (t, *J* = 7.7 Hz, $3H_{Ar(mbz)}$), 4.23 (s, 1H, B-H_t), 4.31 (s, 1H, B-H_t), 3.83 (d, *J* = 10.7 Hz, 9H, OCH_3), -4.13 (br, s, 1H, Ru-*H*-B); $^{13}C\{^1H\}$ NMR (125 MHz, $CDCl_3$, 22°C): δ = 53.6 (OCH_3), 116.7, 120.6, 124.3, 131.7, 140.7, 146.6 (C=N), 195.7, 197.9 (C=S); $^{31}P\{^1H\}$ NMR (121 MHz, $CDCl_3$, 22°C): δ = 136.0; IR (CH_2Cl_2, cm^{-1}): $\tilde{\nu}$ = 2457 (B-H_t), 2028 (B-H_b).

5b: MS (ESI^+): *m/z* calculated for $C_{46}H_{36}RuS_8N_4B_2PO_3$ $[M+H]^+$: 1102.9520, found 1102.9442; $^{11}B\{^1H\}$ NMR (160 MHz, $CDCl_3$, 22°C): δ = -3.3 (br, B1), -6.8 (br, B2); ^1H NMR (500 MHz, $CDCl_3$, 22°C): δ = 7.92 (s, $1H_{Ar(mbz)}$), 7.37–7.30 (m, $4H_{Ar(mbz)}$), 7.22 (t, *J* = 7.9 Hz, $7H_{Ar(mbz)}$), 7.18–7.02 (m, $19H_{Ar(mbz)}$), 7.00 (d, *J* = 8.1 Hz, $5H_{Ar(mbz)}$), 4.38 (s, 3H, B-H_t), -4.44 (br, s, 1H, Ru-*H*-B); $^{13}C\{^1H\}$ NMR (125 MHz, $CDCl_3$, 22°C): δ = 116.6, 120.6, 121.0, 121.7, 124.3, 124.4, 126.5, 129.2, 129.5, 130.0, 131.8, 144.5 (C=N), 145.5 (C=N), 146.5, 151.5, 152.0, 152.6, 152.8 146.6 (C=N), 195.6, (C=S); $^{31}P\{^1H\}$ NMR (121 MHz, $CDCl_3$, 22°C): δ =116.6; IR (CH_2Cl_2, cm^{-1}): $\tilde{\nu}$ =2466 (B-H_t), 2146 (B-H_b).

Synthesis of 6a

To a toluene suspension of compound **5a** (0.050 g, 0.054 mmol) was placed in flammed Schlenk flask and stirred for 12 h at 60 °C. The solvent was removed *in-vacuo* and the residue was dissolved in CH_2Cl_2 (15 mL)/Hexane (5 mL), filtered using Celite. The solvent was removed and the residue was subjected to chromatographic workup using silica-gel TLC plates. Elution with a CH_2Cl_2/hexane(70:30 v/v) mixture yielded red **6a** (30 mg, 61%).

Note that, we have isolated compound **6a** from **3** in very poor yield.

6a: MS (ESI^+): *m/z* calculated for $C_{30}H_{26}RuS_8N_4B_2PO_3$ $[M+H]^+$: 900.8737, found 900.8661; $^{11}B\{^1H\}$ NMR (160 MHz, $CDCl_3$, 22°C): δ = 0.1, -4.6; ^1H NMR (500 MHz, $CDCl_3$, 22°C): δ = 7.82 (d, *J* = 8.4 Hz, $1H_{Ar(mbz)}$), 7.46–7.43 (m, $1H_{Ar(mbz)}$), 7.43–7.39 (m, $1H_{Ar(mbz)}$), 7.37 (dd, *J* = 7.8, 1.3 Hz, $1H_{Ar(mbz)}$), 7.31–7.27 (m, $1H_{Ar(mbz)}$), 7.24 (d, *J* = 3.4 Hz, $1H_{Ar(mbz)}$), 7.19 (t, *J* = 7.6 Hz, $1H_{Ar(mbz)}$), 4.78 (s, 1H, B-H_t), 3.71 (d, *J* = 10.8 Hz, 6H P(OCH_3)$_2$), 3.69 (s, 1H, B-H_t), -3.15 (s, br, 1H, Ru-*H*-B); $^{13}C\{^1H\}$ NMR (125 MHz, $CDCl_3$, 22°C): δ = 53.5, 116.5, 120.3, 121.1, 124.1, 124.6, 126.4, 126.9, 130.9, 132.5, 145.9, 147.4, 195.8.(C=S); $^{31}P\{^1H\}$ NMR (121 MHz, $CDCl_3$, 22°C): δ = 132.3 IR (CH_2Cl_2, cm^{-1}): $\tilde{\nu}$ = 2474 (B-H_t), 2142 (B-H_b), 1032 (P=O).

Synthesis of 7a-b

In a flame dried Schlenk tube, a yellow solution of **3** (0.05 g, 0.063 mmol) and dimethylphenylphosphine (PMe_2Ph) (0.17 mL, 0.119 mmol) in toluene (15 mL) was thermalized for 12 h at 90°C temperature. The volatile components were removed under vacuum and the remaining residue was extracted into CH_2Cl_2/hexane passed through Celite. After removal of solvent, the residue was subjected to chromatographic work up using prepared glass TLC. Elution with a hexane/CH_2Cl_2 (10:90 v/v) yielded yellow **7a** (0.018 g, 31%).

Compound **7b** (0.030g, 54%) is synthesized from reaction of a yellow solution of **3** (0.050 g, 0.063 mmol) and methyldiphenylphosphine (PPh_2Me) (0.25 mL, 0.115 mmol) in toluene (15 mL) under same reaction conditions of **7a**.

Note that under similar reaction conditions, compounds **7a** or **7b** formed with very poor yields from the reaction of **3** with $PR'R_2$ (R and R' = Me or Ph). However, upon increasing the temperature from 60˚C to 90˚C, we obtained moderate yields. This may be due to the strong σ donating and weak π accepting properties of $PR'R_2$ (R and R' = Me or Ph) than $P(OR)_3$ (R = Me or Ph). As a result, we were unable to isolate **5c** and **5d** complexes.

7a: MS (ESI) calcd for *m/z* $C_{37}H_{37}RuS_6N_3BP_2$ $[M+H]^+$: 889.9923, found 889.9925; $^{11}B\{^1H\}$ NMR (160 MHz, $CDCl_3$, 22°C): δ = -2.9 (br, B1); ^1H NMR (500 MHz, $CDCl_3$, 22°C): δ = 7.53 (dd, *J* = 13.4, 5.6 Hz, $3H_{Ar(mbz)}$), 7.49 (s, $1H_{Ar(mbz)}$), 7.47–7.39 (m, $3H_{Ar}$), 7.38–7.33 (m, $3H_{Ar}$), 7.33–7.27 (m, $3H_{Ar}$), 7.24–7.12 (m, $4H_{Ar(mbz)}$), 7.09 (t, *J* = 7.5 Hz, $1H_{Ar}$), 7.06–7.01 (m, $1H_{Ar(mbz)}$), 6.99 (dd, *J* = 14.0, 6.5 Hz, $1H_{Ar(mbz)}$), 6.80 (t, *J* = 7.8 Hz, $1H_{Ar(mbz)}$), 4.44 (br, 1H, s, B-$\underline{H_t}$), 1.78 (dd, *J* = 15.0, 9.2 Hz, 6H), 1.69 (d, *J* = 9.1 Hz, 3H), 1.61 (d, *J* = 9.2 Hz, 3H), -6.93 (s, br, 1H, Ru–*H*–B); $^{13}C\{^1H\}$ NMR (125 MHz, $CDCl_3$, 22 °C): δ = 15.6 (CH_3), 16.4 (CH_3), 16.7 (CH_3), 18.7 (CH_3), 116.0, 116.3, 119.1, 119.7, 120.8, 121.7, 123.7, 123.9, 124.5, 124.7, 125.2, 126.2, 127.2, 127.8, 128.3, 128.6, 129.2, 130.1, 130.3, 132.3, 139.5, 142.0, 144.9 (C=N), 180.9 (C=S), 197.3 (C=S); $^{31}P\{^1H\}$ NMR (121 MHz, $CDCl_3$, 22°C): δ = 21.1 (d, *J* = 36.4 Hz), 12.9 (d, *J* = 36.4 Hz); IR (CH_2Cl_2, cm^{-1}): $\tilde{\nu}$ = 2502 (B-H_t) 2110 (BH_b).

7b: MS (ESI) calcd for *m/z* $C_{47}H_{41}RuS_6N_3BP_2$ $[M+H]^+$: 1014.0236, found 1014.0246; $^{11}B\{^1H\}$ NMR (160 MHz, $CDCl_3$, 22°C): δ = -2.1 (br, B1); ^1H NMR (500 MHz, $CDCl_3$, 22°C); δ = 7.82 (d, *J* = 8.0 Hz, 1H), 7.63 (m, 3H), 7.56 (m, 2H), 7.48 (dt, *J* = 8.6, 2.0 Hz, 4H),

7.34 (d, *J* = 2.2 Hz, 3H), 7.23–7.10 (m, 12H), 7.04–6.95 (m, 5H), 6.91 (dd, *J* = 7.8, 1.5 Hz, 1H), 6.80 (s, $1H_t$), 4.30 (s, $1BH_t$), 2.11 (d, *J* = 8.6 Hz, 3H), 1.80 (d, *J* = 8.8 Hz, 3H), -7.63 (br, 1H, Ru–*H*–B); $^{13}C\{^1H\}$ NMR (125 MHz, $CDCl_3$, 22°C): δ = 15.3(CH_3), 15.6 (CH_3), 115.7, 116.2, 119.2, 119.6, 120.7, 121.2, 121.7, 123.6, 123.8, 124.4, 125.6, 125.9, 126.0, 127.2, 127.3, 127.4, 127.8, 127.9, 128.0, 128.4, 129.0, 129.2, 129.4, 131.6, 131.7, 132.2, 132.3, 145.0; $^{31}P\{^1H\}$ NMR (121 MHz, $CDCl_3$, 22°C): δ = 27.1 (d, *J* = 33.9 Hz), 16.5 (d, *J* = 34.3 Hz); IR (CH_2Cl_2, cm^{-1}): $\tilde{\nu}$ = 2473 (B-H_t), 2087 (B-H_b).

Single-crystal X-ray diffraction analysis

Suitable X-ray quality crystals of **3**, **5a** and **7a** were grown by slow diffusion of a toluene-CH_2Cl_2 solution, other crystals were grown from hexane-CH_2Cl_2 solution. The crystal data of **2, 3** and **7a** were collected and integrated using a D8 VENTURE Bruker AXS diffractometer, with multilayer monochromated Mo Kα (λ = 0.71073 Å) radiation at 150 K. Crystal diffraction data of **4b**, **5a**, **5b**, and **6a** were collected and integrated using a Bruker AXS Kappa APEXII CCD diffractometer with a graphite monochromated Mo-Kα (λ = 0.71073 Å) radiation at 296(2) K. The structures were solved by heavy atom methods using SHELXS-97 or SIR92[34] and refined using SHELXL-2014 or SHELXL-2016.[35] The non-hydrogen atoms were refined with anisotropic displacement parameters. All hydrogens could be located in the difference Fourier map. However, the hydrogen atoms bonded to carbon atoms and boron atoms were fixed at chemically meaningful positions and were allowed to ride with the parent atom during the refinement. The molecular structures were drawn using Olex2.[36] Crystallographic data have been deposited with the Cambridge Crystallographic Data Centre as supplementary publication no CCDC- 1588902 (**2**), 1588858 (**3**), 1890802 (**4b**), 1588859 (**5a**), 1875698 (**5b**), 1890801 (**6a**), 1824575 (**7a**). These data can be obtained free of charge from The Cambridge Crystallographic Data Centre via www.ccdc.cam.ac.uk/data_request/cif.

Crystal data for **2**: $C_{30}H_{23}BCl_2N_4O_2PRuS_8$, M_r = 941.75, Triclinic, space group *P*$\bar{1}$, *a* = 10.3316(8) Å, *b* = 19.1974(15) Å, *c* = 20.2644(17) Å, α = 70.467(3)°, β = 83.562(3)°, γ = 81.359(3)°, *V* = 3736.7(5) $Å^3$, *Z* = 4, ρ_{calcd} = 1.674 g/cm^3, μ = 1.089 mm^{-1}, *F(000)* = 1892, R_1 = 0.0464, wR_2 = 0.1120, 17136 independent reflections [2θ ≤ 50.48°] and 898 parameters.

Crystal data for **3**: $C_{42}H_{32}B_2N_4RuS_8$, M_r = 971.88, Triclinic, space group *P*$\bar{1}$, *a* = 11.1876(11) Å, *b* = 12.1286(14) Å, *c* = 16.999(2) Å, α = 78.891(4)°, β = 71.357(4)°, γ = 73.990(4)°, *V* = 2087.0(4) $Å^3$, *Z* = 2, ρ_{calcd} = 1.547g/cm^3, μ = 0.814 mm^{-1}, *F(000)* = 988, R_1 = 0.0811, wR_2 = 0.2037, 9471 independent reflections [2θ ≤ 50.48°] and 511 parameters.

Crystal data for **4b**: $C_{39}H_{29}BN_3O_3RuPS_6$, M_r = 922.86, Monoclinic, space group $P2_1/n$, *a* = 15.6837(17) Å, *b* = 17.7045(18) Å, *c* = 16.1046(17) Å, α = 90°, β = 112.312(4)°, γ = 90°, *V* = 4137.0(8) $Å^3$, *Z* = 4, ρ_{calcd} = 1.482 g/cm^3, μ = 0.761 mm^{-1}, *F(000)* = 1872, R_1 = 0.0939, wR_2 = 0.2577, 9343 independent reflections [2θ ≤ 50.48°] and 488 parameters. The poor quality of the measured crystal and the collected X-ray diffraction data affect the value of R1, providing large residual electronic densities and leading to remaining B-type alerts.

Crystal data for **5a**: $C_{32}H_{31}B_2Cl_2N_4O_3PRuS_8$, M_r = 1000.65, Orthorhombic, space group $P2_12_12$, *a* = 12.5101(8) Å, *b* = 28.6346(17) Å, *c* = 11.2355(8) Å, α = 90°, β = 90°, γ = 90°, *V* = 4024.8(5) $Å^3$, *Z* = 4, ρ_{calcd}= 1.651g/cm^3, μ = 1.018 mm^{-1}, *F(000)* = 2024, R_1 = 0.0438, wR_2 = 0.0906, 8778 independent reflections [2θ ≤ 50.48°] and 481 parameters.

Crystal data for **5b**: $C_{46}H_{35}B_2N_4O_3PRuS_8$, M_r = 1101.92, Monoclinic, space group $P2_1/n$, *a* = 12.4288(13) Å, *b* = 19.548(2) Å, *c* = 20.620(2) Å, α = 90°, β = 107.085(3)°, γ = 90°, *V* = 4788.6(9) $Å^3$, *Z* = 4, ρ_{calcd} = 1.528 g/cm^3, μ = 0.756 mm^{-1}, *F(000)* = 2240, R_1 = 0.0451, wR_2 = 0.0825, 8448 independent reflections [2θ ≤ 50°] and 678 parameters.

Crystal data for **6a**: $C_{63}H_{56}B_4Cl_6N_8O_6P_2Ru_2S_{16}$, M_r = 2054.13, Monoclinic, space group *C2/c*, *a* = 40.711(2) Å, *b* = 10.3815(5) Å, *c* = 38.999(3) Å, α = 90°, β = 102.745(2)°, γ = 90°, *V* = 16076.4(16) $Å^3$, *Z* = 8, ρ_{calcd} = 1.697 g/cm^3, μ = 1.086 mm^{-1}, *F(000)* = 8272, R_1 = 0.0650, wR_2 = 0.1265, 11974 independent reflections [2θ ≤ 47.18°] and 992 parameters.

Crystal data for **7a**: $C_{44}H_{44}BN_3P_2RuS_6$, M_r = 981.00, Triclinic, space group *P*$\bar{1}$, *a* = 11.5518(9) Å, *b* = 13.5810(12) Å, *c* = 15.0366(14) Å, α = 107.628(3) °,β = 99.476(3)°, γ = 98.850(3)°, *V* = 2164.9(3) $Å^3$, Z = 2, ρ_{calcd} = 1.505 g/cm^3, μ = 0.762 mm^{-1}, F(000) = 1848, R_1 = 0.0299, wR_2 = 0.0647, 9829 independent reflections [2θ ≤ 50.48°] and 488 parameters.

Computational details

Geometry optimization of all molecules were carried out using the Gaussian 09 program package.[37] Optimization was conducted in the gaseous state (no solvent effect) without any symmetry constraints using the PBE1PBE (PBE0) functional with the combination of the def2-TZVP basis set for all the atoms.[38] The 28 core electrons of ruthenium were replaced by quasi-relativistic def2-ECP effective core potentials.[39] Frequency calculations were performed at the same level of theory. The absence of any imaginary frequencies confirmed that all structures are minima on the potential energy hypersurfaces. The gauge-including atomic orbitals (GIAOs)[40] method has been employed to compute NMR chemical shifts with hybrid Becke–LeeYangParr (B3LYP) functional[41] using optimized geometries at the PBE0/def2-TZVP level. ^{11}B NMR chemical shifts were calculated relative to B_2H_6 (B shielding constant 83.6 ppm) and transformed to the usual [$BF_3.OEt_2$] scale using the experimental $\delta(^{11}B)$ value of B_2H_6, 16.6 ppm. TMS ($SiMe_4$) was used as the internal standards for the ^1H NMR chemical shift calculations. Natural bonding analyses were performed using the natural bond orbital (NBO) 6.0 program.[42] Wiberg bond indices (WBI)[43] were obtained from these natural bond orbital analyses. The two dimensions of the Laplacian electron density plots were obtained using the Multiwfn V.3.3.8 package.[44] Orbital graphics and optimized structure plots were generated by with Jmol 14.0.10[45] and Chemcraft.[46]

Conflicts of interest

There are no conflicts to declare.

Acknowledgements

This work was supported by SERB (Project No. EMR/2015/001274), New Delhi, India. MZ and KP thank IIT Madras for research fellowships. RR thanks the University Grants Commission (UGC), India, for a fellowship. IIT Madras is gratefully acknowledged for computational facilities.

Notes and references

‡ All our attempts to isolate the analogues of **5** with PPh_3 or PCy_3 ligands were unsuccessful maybe due to steric and electronic factors.

1 (a) R. H. Crabtree, *The Organometallic Chemistry of the Transition Metals,* 4th ed., Wiley-Interscience: Hoboken, NJ, 2005; pp 99−103; (b) C. A. Tolman, *Chem. Rev.*, 1977, **77**, 313–348; (c) K. A. Bunten, L. Chen, A. L. Fernandez and A. J. Poe, *Coord. Chem. Rev.*, 2002, **233–234**, 41–51.

2 (a) D. G. Gilheany, *Structure and Bonding in Organophosphorus-(III) Compounds. In The Chemistry of Organophosphorus Compounds;* F. R. Hartley, Ed.; John Wiley & Sons: New York, 1990; vol. 1, pp 9–49; (b) O. Kuehl, *Coord. Chem. Rev.*, 2005, **249**, 693–704; (c) Z. Freixa and P. W. N. M. van Leeuwen, *Dalton Trans.*, 2003, 1890–1901.

3 (a) J. H. Downing and M. B. Smith*, In Comprehensive Coordination Chemistry II,* Elsevier: Amsterdam, The Netherlands, 2004; vol. 1, pp 253–296; (b) T. Leyssens, D. Peeters, A. G. Orpen and J. N. Harvey, *Organometallics*, 2007, **26**, 2637–2645; (c) G. C. Fortman and S. P. Nolan, *Organometallics*, 2010, **29**, 4579–4583.

4 (a) P. W. N. M. van Leeuwen, Z. Freixa and E. Zuidema, *Phosphorus Ligands in Asymmetric Catalysis,* Wiley-VCH: Weinheim, Germany, 2008, vol. 3, pp 1433–1454; (b) J. F. Hartwig, *Organotransition Metal Chemistry: from Bonding to Catalysis*. University Science Books: Herndon, VA, 2010; pp 32–38; (c) D. H. Valentine, J. H. Hillhouse, *Synthesis* 2003, 317–334; (d) M. R. Biscoe, T. E. Barder, S. L. Buchwald, *Angew. Chem. Int. Ed.,* 2007, **46**, 7232–7235.

5 S. T. Diver, In *Encyclopedia of Reagents for Organic Synthesis*, L.A. Paquette (Ed.), Wiley, New York, 1995, vol. 7, pp 5014–5016.

6 (a) P. W. N. M. van Leeuwen, C. F. Roobeek, R. L. Wife, J. H. G. Frijns, *J. Chem. Soc., Chem. Commun*., 1986, 31–33; (b) P. W. N. M. van Leeuwen and C. F. Roobeek, *Eur. Pat. Appl.,* EP 82576, 1983, *Chem. Abstr.,* 1983, **99**, 121813.

7 (a) M. J. Gallagher, *The Chemistry of the Organophosphorus Compounds*, F. R. Hartley (Ed.): Wiley, New York, 199, vol. 2; (b) A. Christiansen, C. Li, M. Garland, D. Selent, R. Ludwig, A. Spannenberg, W. Baumann, R. Franke and A. Börner, *Eur. J. Org. Chem.*, 2010, 2733–2741.

8 (a) D. Martin, D. Moraleda, T. Achard, L. Giordano and G. Buono, *Chem. Eur. J.*, 2011, **17**, 12729–12740; (b) N. V. Dubrovina and A. Börner, *Angew. Chem., Int. Ed.*, 2004, **43**, 5883–5886.

9 (a) V. S. Nacianceno, L. Ibarlucea, C. Mendicute-Fierro, A. Rodríguez-Dieguez, J. M. Seco, A. J. Mota and M. A. Garralda, *Inorg. Chem.*, 2018, **57**, 5307–5319; (b) H. Landert, F. Spindler, A. Wyss, H.-U. Blaser, B. Pugin, Y. Ribourduoille, B. Gschwend, B. Ramalingam and A. Pfaltz, *Angew. Chem. Int. Ed.*, 2010, **49**, 6873–6876; (c) R. Lhermet, E. Moser, E. Jeanneau, H. O.-Bourbigou and P.-A. R. Breuil, *Chem. Eur. J.,* 2017, **23**, 7433–7437; (d) A. Christiansen, D. Selent, A. Spannenberg, W. Baumann, R. Franke and A. Börner, *Organometallics*, 2010, **29**, 3139–3145; (e) R. G.-Fernández, P. J. G.-Liste, J. Borge, P. Crochet and V. Cadierno, *Catal. Sci. Technol.*, 2016, **6**, 4398– 4409; (f) E. Y. Y. Chan, Q.-F. Zhang, Y.-K. Sau, S. M. F. Lo, H. H. Y. Sung, I. D. Williams, R. K. Haynes and W.-H. Leung, *Inorg. Chem.*, 2004, **43**, 4921–4926; (g) M. Liniger, B. Gschwend, M. Neuburger, S. Schaffner and A. Pfaltz, *Organometallics*, 2010, **29**, 5953–5958.

10 (a) S. M. M. Knapp, T. J. Sherbow, R. B. Yelle, J. J. Juliette and D. R. Tyler, *Organometallics*, 2013, **32**, 3744–3752; (b) C. J. den Reijer, M. Wörle and P. S. Pregosin, *Organometallics*, 2000, **19**, 309–316.

11 L. V. Graux, M. Giorgi, G. Buono and H. Clavier, *Organometallics*, 2015, **34**, 1864–1871.

12 I. W. Robertson and T. A. Stephenson, *Inorg. Chim. Acta*, 1980, **45**, L215–L216.

13 (a) X. Tan, W. Zeng, X. Zhang, L. W. Chung and X Zhang, *Chem. Commun.*, 2018, **54**, 535–538; (b) R. Menye-B27iyogo, F. Delpech, A. Castel, H. Gornitzka, and P. Rivière, *Angew. Chem. Int. Ed.,* 2003, **42**, 5610–5612.

14 (a) T. M. Douglas, A. B. Chaplin, A. S. Weller, X. Yang and M. B. Hall, *J. Am. Chem. Soc.*, 2009, **131**, 15440–15456; (b) M. A. Rankin, K. D. Hesp, G. Schatte, R. McDonald and M. Stradiotto, *Dalton Trans.*, 2009, 4756–4765.

15 (a) G. Alcaraz and S. Sabo-Etienne, *Angew. Chem. Int. Ed.*, 2010, **49**, 7170–7179; Y. Gloaguen, G. Alcaraz, L. Vendier, S. Sabo-Etienne, *J. Organomet. Chem.*, 2009, **694**, 2839–2841; (c) G. R. Owen, *Chem. Soc. Rev*., 2012, **41**, 3535–3546; (d) T. Stahl, K. Müther, Y. Ohki, K. Tatsumi and M. Oestreich, *J. Am. Chem. Soc.*, 2013, **135**, 10978–10981; (e) M. W. Drover, E. G. Bowes, L. L. Schafer, J. A. Love and A. S. Weller, *Chem. Eur. J.*, 2016, **22**, 6793–6797.

16 (a) I. A. I. Mkhalid, J. H. Barnard, T. B. Marder, J. M. Murphy and J. F. Hartwig, *Chem. Rev.*, 2010, **110**, 890–931; (b) M. W. Drover, L. L. Schafer and J. A. Love, *Angew. Chem. Int. Ed.,* 2016, **55**, 3181–3186.

17 R. Kumar and B. R. Jagirdar, *Inorg. Chem.*, 2013, **52**, 28–36.

18 (a) M. Shimoi, S. Nagai, M. Ichikawa, Y. Kawano, K. Katoh, M. Uruichi and H. Ogino, *J. Am. Chem. Soc.*, 1999, **121**, 11704–11712; (b) A. Kumar, H. C. Johnson, T. N. Hooper, A. S. Weller, A. G. Algarra and S. A. Macgregor, *Chem. Sci.*, 2014, **5**, 2546–2553; (c) J. B. Geri, N. K. Szymczak, *J. Am. Chem. Soc.,* 2015, **137**, 12808–12814.

19 (a) S. Schlecht and J. F. Hartwig, *J. Am. Chem. Soc.*, 2000, **122**, 9435–9443; (b) G. Alcaraz, E. Clot, U. Helmstedt, L. Vendier and S. Sabo-Etienne, *J. Am. Chem. Soc.*, 2007, **129**, 8704–8705; (c) K. D. Hesp, F. O. Kannemann, M. A. Rankin, R. McDonald, M. J. Ferguson, M. Stradiotto, *Inorg. Chem.,* 2011, **50**, 2431–2444.

20 (a) R. S. Anju, D. K. Roy, B. Mondal, K. Yuvaraj, C. Arivazhagan, K. Saha, B. Varghese and S. Ghosh, *Angew. Chem. Int. Ed.*, 2014, **53**, 2873–2877; (b) D. K. Roy, B. Mondal, R. S. Anju and S. Ghosh, *Chem. Eur. J.*, 2015, **21**, 3640–3648; (c) K. Saha, B. Joseph, R. Ramalakshmi, R. S. Anju, B. Varghese and S. Ghosh, *Chem. Eur. J.*, 2016, **22**, 7871–7878; (d) K. Bakthavachalam, K. Yuvaraj, M. Zafar and S. Ghosh, *Chem. Eur. J.*, 2016, **22**, 17291–17297.

21 (a) D. K. Roy, R. Borthakur, S. Bhattacharyya, V. Ramkumar and S. Ghosh, *J. Organomet. Chem.*, 2015, **799-800**, 132–140; (b) R. Ramalakshmi, K. Saha, D. K. Roy, B. Varghese, A. K. Phukan and S. Ghosh, *Chem. Eur. J.*, 2015, **21**, 17191–17195; (c) K. Saha, R. Ramalakshmi, S. Gomosta, K. Pathak, V. Dorcet, T. Roisnel, J.-F. Halet and S. Ghosh, *Chem. Eur. J.*, 2017, **23**, 9812–9820; (d) R. Ramalakshmi, K. Maheswari, D. Sharmila, A. Paul, T. Roisnel, J.-F. Halet and S. Ghosh, *Dalton Trans.*, 2016, **45**, 16317–16324.

22 E. Tomás-Mendivil, F. L. Suárez, J. Diez and V. Cadierno, *Chem. Commun.*, 2014, **50**, 9661–9664.
23 A. Cassen, Y. Gloaguen, L. Vendier, C. Duhayon, A. Pobladór-Bahamonde, C. Raynaud, E. Clot, G. Alcaraz and S. Sabo-Etienne, *Angew. Chem. Int. Ed.*, 2014, **53**, 7569–7573.
24 (a) S. Ghosh, B. C. Noll and T. P. Fehlner, *Angew. Chem. Int. Ed.*, 2005, **44**, 6568–6571; (b) K. Geetharani, S. K. Bose, S. Sahoo, B. Varghese, S. M. Mobin, and S. Ghosh, *Inorg. Chem.,* 2011, **50**, 5824–5832; (c) K. Yuvaraj, D. K. Roy, K. Geetharani, B. Mondal, V. P. Anju, P. Shankhari, V. Ramkumar and S. Ghosh, *Organometallics*, 2013, **32**, 2705–2712; (d) S. Ghosh, T. P. Fehlner and B. C. Noll, *Chem. Commun.*, 2005, 3080–3082; (e) R. S. Anju, K. Saha, B. Mondal, V. Dorcet, T. Roisnel, J.-F. Halet and S. Ghosh, *Inorg. Chem.,* 2014, **53**, 10527–10535; (f) R. S. Anju, D. K. Roy, K. Geetharani, B. Mondal, B. Varghese and S. Ghosh, *Dalton Trans.,* 2013, **42**, 12828–12831; (g) S. K. Bose, D. K. Roy, P. Shankhari, K. Yuvaraj, B. Mondal, A. Sikder, and S. Ghosh, *Chem. Eur. J.,* 2013, **19**, 2337 –2343.
25 D. J. Harding, H. Adams and T. Tuntulani, *Acta Cryst.,* 2005, **C61**, m301–m303.
26 A. Phanopoulos, N. J. Long, and P. W. Miller, *Struct. Bond.,* 2016, **171**, 31–61.
27 (a) E. E. Joslin, C. L. McMullin, T. B. Gunnoe, T. R. Cundari, M. Sabat and W. H. Myers, *Inorg. Chem.*, 2012, **51**, 4791–4801; (b) E. E. Joslin, B. Quillian, T. B. Gunnoe, T. R. Cundari, M. Sabat and W. H. Myers, *Inorg. Chem.*, 2014, **53**, 6270–6279.
28 (a) R. Lhermet, E. Moser, E. Jeanneau, H. O. Bourbigou and P.-A. R. Breuil, *Chem. Eur. J.*, 2017, **23**, 7433–7437; (b) J. A. Bailey, H. A. Sparkes and P. G. Pringle, *Chem. Eur. J.*, 2015, **21**, 5360–5363; (c) Kölle, T. Rüther, N. Le Narvor, U. Englert and W. Kläui, *Angew. Chem. Int. Ed.*, 1994, **33**, 991–993.
29 (a) R. Prakash, A. De, K. Bakthavachalam and S. Ghosh, *Inorg. Chem.*, 2018, **57**, 14748–14757; (b) D. Zhu, J. H. W. LaFortune, R. L. Melen and D. W. Stephan, *Dalton Trans.*, 2019, 10.1039/C8DT04818E.
30 E. Tomás-Mendivil, V. Cadierno, M. I. Menéndez and R. López, *Chem. Eur. J.*, 2015, **21**, 16874–16886.
31 M. Imran, B. Neumann, H.-G. Stammler, U. Monkowius, M. Ertl and N. W. Mitzel, *Dalton Trans.*, 2014, **43**, 1267–1278.
32 G. E. Ryschkewitsch and K. C. Nainan, *Inorg. Synth.,* 1975, **15**, 11–15.
33 (a) J. J. Led and H. Gesmar, *Chem. Rev.*, 1991, **91**, 1413–1426; (b) L. Yang, R. Simionescu, A. Lough and H. Yan, *Dyes Pigm.*, 2011, **91**, 264–267.
34 A. Altomare, M. C. Burla, M. Camalli, G. L. Cascarano, C. Giacovazzo, A. Guagliardi, A. G. G. Moliterni, G. Polidori and R. Spagna, *J. Appl. Crystallogr.*, 1999, **32**, 115–119.
35 (a) G. M. Sheldrick, *Acta Cryst. Sect. A*, 2015, **71**, 3–8; (b) G. M. Sheldrick, *Acta Cryst. Sect. C*, 2015, **71**, 3–8.
36 O. V. Dolomanov, L. J. Bourhis, R. J. Gildea, J. A. K. Howard and H. Puschmann, *J. Appl. Cryst.,* 2009, **42**, 339–341.
37 *Gaussian 09, Revision C.01,* M. J. Frisch, G. W. Trucks, H. B. Schlegel, G. E. Scuseria, M. A. Robb, J. R. Cheeseman, G. Scalmani, V. Barone, B. Mennucci, G. A. Petersson, H. Nakatsuji, M. Caricato, X. Li, H. P. Hratchian, A. F. Izmaylov, J. Bloino, G. Zheng, J. L. Sonnenberg, M. Hada, M. Ehara, K. Toyota, R. Fukuda, J. Hasegawa, M. Ishida, T. Nakajima, Y. Honda, O. Kitao, H. Nakai, T. Vreven, J. A. Montgomery, Jr., J. E. Peralta, F. Ogliaro, M. Bearpark, J. J. Heyd, E. Brothers, K. N. Kudin, V. N. Staroverov, T. Keith, R. Kobayashi, J. Normand, K. Raghavachari, A. Rendell, J. C. Burant, S. S. Iyengar, J. Tomasi, M. Cossi, N. Rega, J. M. Millam, M. Klene, J. E. Knox, J. B. Cross, V. Bakken, C. Adamo, J. Jaramillo, R. Gomperts, R. E. Stratmann, O. Yazyev, A. J. Austin, R. Cammi, C. Pomelli, J. W. Ochterski, R. L. Martin, K. Morokuma, V. G. Zakrzewski, G. A. Voth, P. Salvador, J. J. Dannenberg, S. Dapprich, A. D. Daniels, O. Farkas, J. B. Foresman, J. V. Ortiz, J. Cioslowski and D. J. Fox, Gaussian, Inc., Wallingford CT, 2010.
38 J. P. Perdew, K. Burke and M. Ernzerhof, *Phys. Rev. Lett.*, 1996, **77**, 3865–3868.
39 D. Andrae, U. Häußermann, M. Dolg, H. Stoll and H. Preuss, *Theor. Chim. Acta*, 1990, **77**, 123–141.
40 (a) F. J. London, *J. Phys. Radium*, 1937, **8**, 397–409; b) R. Ditchfield, *Mol. Phys.*, 1974, **27**, 789–807; c) K. Wolinski, J. F. Hinton and P. Pulay, *J. Am. Chem. Soc.*, 1990, **112**, 8251–8260.
41 C. Lee, W. Yang and R. G. Parr, *Phys. Rev.* B., 1988, **37**, 785–789.
42 *NBO Program 6.0,* E. D. Glendening, J. K. Badenhoop, A. E. Reed, J. E. Carpenter, J. A. Bohmann, C. M. Morales, C. R. Landis, F. Weinhold, Theoretical Chemistry Institute, University of Wisconsin, Madison, WI, 2013.
43 K. Wiberg, *Tetrahedron*, 1968, **24**, 1083–1096.
44 T. Lu, F. Chen, *J. Comput. Chem.,* 2012, **33**, 580–592.
45 Jmol: an open-source Java viewer for chemical structures in 3D. http://www.jmol.org/
46 Chemcraft: Graphical software for visualization of quantum chemistry computations. https://www.chemcraftprog.com.

Table of Content Entry Only

Mercapto-benzothiazolyl based ruthenium(II) borate complexes: Synthesis and reactivity towards various phosphines

Mohammad Zafar,[a] Rongala Ramalakshmi,[a] Alaka Nanda Pradhan[a], Kriti Pathak,[a] Thierry Roisnel,[b] Jean-François Halet,[b] Sundargopal Ghosh*[a]

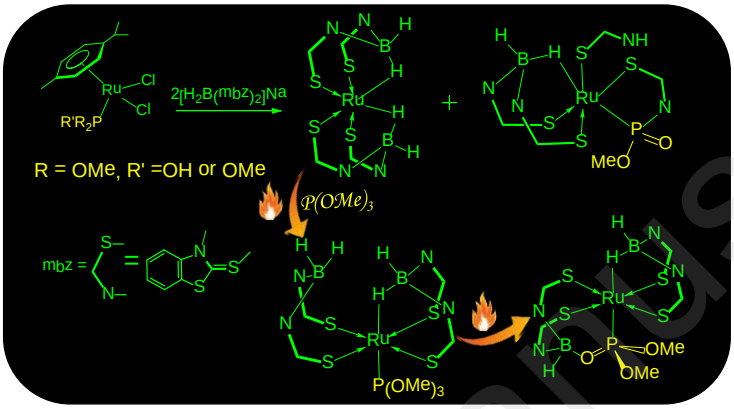

Ruthenium complexes featuring phosphinate and dual Ru···H-B interactions between Ru and B-H bonds of borate ligands supported by mercapto-benzothiazolyl heterocycles have been synthesized. The flexible nature of Ru···H-B interactions in one of the characterized complexes is demonstrated by their reactivity towards phosphite and phophine ligands.